Eur. Phys. J. Special Topics **227**, 1501–1514 (2019)

https://doi.org/10.1140/epjst/e2019-800152-6

THE EUROPEAN PHYSICAL JOURNAL SPECIAL TOPICS

Regular Article

Fully implicit time integration in truly incompressible SPH

Manuel Hopp-Hirschler[a] and Ulrich Nieken

Institute of Chemical Process Engineering, University of Stuttgart, Böblinger Straße 78, 70199 Stuttgart, Germany

Received 27 September 2018 / Received in final form 21 November 2018
Published online 8 March 2019

Abstract. In the last years, the Smoothed Particle Hydrodynamics (SPH) method was introduced in new fields of engineering applications where highly viscous flow like polymer flow or very small geometries, like in micro-flow, are involved. In most of these applications it was not possible to use realistic fluid parameters, larger simulation domains or higher resolution because of restriction of time step due to the viscous time step criterion of the explicit time integration scheme. The computational effort was too high even for highly scalable SPH codes. In this article, we present a first-order implicit time stepping scheme for truly incompressible SPH (ISPH) to eliminate the viscous time step criterion. We propose a consistent time stepping approach where both velocity and particle position are solved implicitly and compare the results to traditional semi-implicit ISPH and implicit schemes where only velocity is integrated implicitly. We study Poiseuille flow, Taylor–Green flow and Rayleigh–Taylor instability and compare results of the implicit schemes to ISPH. Energy conservation is investigated using Taylor–Green vortex to highlight differences between the approaches. We find that the fully implicit time integration scheme is numerically stable. Since no error estimation of accuracy is used, the larger time step size leads to deviations of the trajectories. In future work, higher-order time integration schemes as well as error estimators should be investigated.

1 Introduction

In the last years Smoothed Particle Hydrodynamics (SPH) [1,2] became popular in engineering applications. Beside the major area of ocean and marine engineering, SPH is applied in real-life applications like molding flow and micro-flow in porous media [3–6]. In the latter areas the numerical efficiency is restricted by the viscous stability criterion of the explicit time stepping scheme, e.g. explicit Euler or Runge–Kutta scheme, because of low Reynolds numbers due to large viscosity and/or small geometries. As a result simulated real-times are relatively small and therefore it is impossible to match the experimental time scale.

[a] e-mail: manuel.hopp@icvt.uni-stuttgart.de

There exist different solutions in literature to overcome this shortcoming. For example, one may use an adaptive resolution of the computational domain to reduce the computational cost and only resolve parts of major interest in detail [7–10]. Alternatively, one may use a multi-scale approach to enable an efficient solution of the experimental time-scale [11]. In general, we lose some details but cover the major characteristics and it may be sufficient for real-life applications.

Another solution to overcome small time steps is an implicit time integration scheme. This may enable larger time steps because the time step restricting viscous stability criterion in micro-flow problems vanishes. Implicit time integration schemes are iterative schemes. Since in truly incompressible SPH (ISPH) [12] a system of linear equations is solved already, the additional computational cost may be low.

In general, implicit time integration in the context of incompressible Navier–Stokes flow was discussed in detail in many textbooks. In ISPH, we typically use a predictor-corrector scheme where in the corrector step a Pressure Poisson Equation (PPE) is solved to estimate the pressure in the system. This scheme is semi-implicit because the predictor step is typically an explicit step while the corrector step is implicit. The limiting time step depends on the predictor step. Therefore, larger time steps may be possible if the predictor step is implicit too. In this way it is similar to a segregated approach in grid-based methods.

In the context of SPH, implicit time integration was mainly discussed for weakly compressible SPH (WCSPH), where in contrast to ISPH the pressure is evaluated using an equation of state. Monaghan [13] first introduced implicit time integration for the drag force between fluids. Litvinov et al. [14] introduced a splitting integration scheme in Smoothed Dissipative Particle Dynamics (SDPD) [15] to separately integrate conservative forces, dissipative (viscous) and random forces. The latter forces are integrated implicitly. In both integration schemes, they account for the position of particles in future time by updating the velocity for each pair of interacting particles iteratively.

Fan et al., Han et al., Takahashi et al. and Weiler et al. [16–20] used implicit time integration for the viscous force in the Navier–Stokes equations to overcome the viscous time step limitation for integration of the velocity. Ihmsen et al. [21] used an implicit scheme to compute the pressure. This approach was further improved for high performance computing by different groups [22,23]. Rook et al. [24] used an implicit time integration scheme for scalar transport, e.g. temperature, where particles are fixed in the domain. In the limit of negligible inertia forces (low Reynolds numbers) or in the limit of very large time steps, e.g. in steady-state flow fields, Liedekerke et at. [25] introduced an integration scheme for Stokes flow that differs from the implicit integration scheme only in the time derivative of the velocity. In all approaches, the position of particles in future time is not considered and therefore implicitly assumed that particle configuration is constant.

Very recently, Pan et al. [26] introduced an implicit time integration scheme for ISPH. In the predictor-corrector scheme, the intermediate velocity in the predictor step is implicitly calculated where the pressure term of the last time step is considered. After solving a Pressure Poisson Equation for the increment of the pressure between two time steps, the pressure is corrected to account for the position of particles in future time. Unfortunately, they didn't show a detailed discussion and limitations of the implicit time integration scheme for complex flow problems.

In this article, we propose a first-order fully implicit time integration scheme for ISPH. The velocity and particle positions are implicitly integrated using a linear equation system for velocity enclosed by a fixed point iteration for particle position. We investigate the proposed time integration scheme by studying different single-phase and multi-phase flow problems and compare results to semi-implicit ISPH and implicit schemes where only velocity is integrated implicitly.

The article is organized as follows: First we present the governing equations and its discrete formulation using SPH. Then we introduce different implicit time integration schemes and investigate simple Poiseuille flow, Rayleigh–Taylor instability and Taylor–Green vortex.

2 Model

2.1 Governing equations

We consider the isotherm incompressible Navier–Stokes equations

$$\rho \frac{D\mathbf{u}}{Dt} = -\nabla p + \mu \Delta \mathbf{u} + \mathbf{F}. \tag{1}$$

$$\nabla \cdot \mathbf{u} = 0. \tag{2}$$

ρ, $\mathbf{u}$, p and μ are the density, velocity, pressure and dynamic viscosity. The body force

$$\mathbf{F} = \rho \mathbf{g} + \mathbf{F}_{\text{surf}} \tag{3}$$

consists of the gravitational force $\rho\mathbf{g}$ and the surface tension force $\mathbf{F}_{\text{surf}}$. We assume the sharp interface limit and use

$$\mathbf{F}_{\text{surf}} = \sigma \kappa \hat{\mathbf{n}} \delta_{\text{surf}} \tag{4}$$

with the surface tension coefficient σ, the curvature of the interface κ, the unit normal $\hat{\mathbf{n}}$ and the Dirac-function δ_{surf} that is unity at the interface and zero elsewhere.

2.2 Discrete equations

We discretize the governing equations using the Smoothed Particle Hydrodynamics method, which is a Lagrangian mesh-free discretization method, where a quantity is approximated by integrating neighboring interpolation points (so-called particles) in the surrounding volume. A general introduction and derivation of the discrete operators are found in the reviews of Monaghan [27] and Liu & Liu [28]. The present model is based on the previous work of Hirschler et al. [5]. We briefly summarize the discrete balance equations and refer to [5] for further reading.

We use the discrete continuity equation

$$\rho_i = m_i \sum_j W\left(|\mathbf{r}_{ij}|, h\right). \tag{5}$$

m_i, $|\mathbf{r}_{ij}|$ and h are the mass of particle i, the distance between particle i and j and the smoothing length. We use a Wendland C2 kernel and $h = 2.05 L_0$ with an initial particle distance L_0. In the following, $W_{ij} = W\left(|\mathbf{r}_{ij}|, h\right)$.

The discrete Navier–Stokes equation is

$$\begin{aligned} \frac{D\mathbf{u}_i}{Dt} = &- \sum_j \frac{m_j}{\rho_i \rho_j} \left(p_i + p_j\right) \tilde{\nabla} \tilde{W}_{ij} \\ &+ \sum_j \frac{m_j \left(\mu_i + \mu_j\right)}{\rho_i \rho_j} \frac{\mathbf{r}_{ij}}{|\mathbf{r}_{ij}|^2} \tilde{\nabla} \tilde{W}_{ij} \cdot \left(\mathbf{u}_i - \mathbf{u}_j\right) \\ &+ \mathbf{g}_i + \frac{\sigma_i}{\rho_i} \kappa_i \mathbf{n}_i. \end{aligned} \tag{6}$$

$\tilde{\nabla}\tilde{W}_{ij}$ is the corrected gradient of the corrected kernel function as introduced by Bonet & Lok [29] to account for kernel consistency. We use the continuum surface force (CSF) model [30] in the last term of equation (6). Herein, $\mathbf{n}_i$ is the non-unit normal

$$\mathbf{n}_i = \sum_j \frac{m_j}{\rho_j} \frac{(C_j - C_i)}{[C]} \nabla W_{ij}. \tag{7}$$

C_i and $[C]$ are the color function of particle i and its jump across the interface. The curvature of particle i is

$$\kappa_i = -\sum_j \frac{m_j}{\rho_j} \left(\hat{\mathbf{n}}_j - \hat{\mathbf{n}}_i\right) \tilde{\nabla}\tilde{W}_{ij}. \tag{8}$$

$\hat{\mathbf{n}}_i$ is the unit normal of particle i. Note that in equation (8) only particles with a normal greater than $0.01/h$ are considered.

2.3 Pressure

In ISPH, a projection method (predictor-corrector scheme) is used to estimate the pressure in the system [12,31]. Therefore, a Pressure Poisson Equation (PPE) needs to be solved. According to the continuity equation (Eq. (2)), the PPE is written as

$$\nabla \cdot \left(\frac{1}{\rho}\nabla p\right)_i = \frac{\nabla \cdot \mathbf{u}_i^*}{\Delta t} \tag{9}$$

where incompressibility is defined by a divergence-free velocity field. $\mathbf{u}_i^*$ is the intermediate velocity of particle i after the predictor step. Δt is the time step size. We use the discrete formulation

$$\sum_j 2\frac{m_j}{\rho_i \rho_j} \cdot \left(p_i - p_j\right) \frac{\mathbf{r}_{ij}}{r_{ij}^2} \tilde{\nabla}\tilde{W}_{ij} = \frac{1}{\Delta t} \sum_j \frac{m_j}{\rho_j} \left(\mathbf{u}_j^* - \mathbf{u}_i^*\right) \tilde{\nabla}\tilde{W}_{ij}. \tag{10}$$

Further details are found in [5].

The system of linear equations (LES) is solved using the algebraic multigrid preconditioner *boomerAMG* from the hypre library [32] with default configuration except for the number of iterations set to 5 instead of 1 and a *BiCGStab* solver from the PETSc library [33].

2.4 Particle shifting approach

A consistent particle density and particle distribution is important for stable and accurate simulations. We use the particle shifting technique introduced by Xu et al. [34]. Near a fluid interface we use the extension introduced by Lind et al. [35] and only shift in tangential direction to the interface.

2.5 Boundary conditions

We use mirror particle boundary conditions. At solid walls no-slip conditions are applied to velocity and Neumann boundary conditions are applied for pressure. At inflow/outflow boundary conditions, pressure is specified and zero divergence of velocity is assumed. Both techniques are described in detail in [5,36] and represent current state-of-the-art technique.

3 Time stepping

In this section, we first review the predictor-corrector scheme commonly used in ISPH. Then, we introduce two implicit time integration schemes for ISPH; one for implicit time integration of the velocity of particles only (s-IISPH), as e.g. in [16], and a fully implicit time integration scheme for velocity and position of particles (f-IISPH).

3.1 ISPH

In the projection scheme, equation (6) is divided into a curl-free and divergence-free part. The curl-free part includes the viscous term and all body forces, including surface tension. The divergence-free part consists of the pressure term only. In a time step, the curl-free part is used to calculate an intermediate velocity of each particle

$$\mathbf{u}_i^{*,t+\Delta t} = \mathbf{u}_i^{t,x^t} + \left[\frac{1}{\rho_i}\left(\mu\Delta\mathbf{u} + \mathbf{F}\right)_i\right]^{t,x^t} \Delta t. \tag{11}$$

The indices indicate the time and position in time at which velocity and forces are calculated. t and $t+\Delta t$ are the time at the beginning and end of a time step. Usually, an explicit Euler (as in this article) or leap frog [37] time step is used in the predictor step.

Next, a PPE (Eq. (10)) is solved to estimate a pressure which ensures incompressibility. Finally, the intermediate velocity is corrected

$$\mathbf{u}_i^{t+\Delta t} = \mathbf{u}_i^{*,t+\Delta t} - \left(\frac{1}{\rho}\nabla p\right)_i^{t+\Delta t,x^t} \Delta t. \tag{12}$$

At the end, the position of particles is updated

$$\mathbf{x}_i^{t+\Delta t} = \mathbf{x}_i^t + \frac{\mathbf{u}_i^t + \mathbf{u}_i^{t+\Delta t}}{2}\Delta t \tag{13}$$

using a second-order step. Since intermediate velocity and position are updated explicitly, the time step is limited. We use the stability criteria for convective transport

$$\Delta t_{\mathrm{CFL}} = \alpha_{\mathrm{CFL}}\frac{L_0}{u_{\max}}, \tag{14}$$

with $\alpha_{\mathrm{CFL}} = 0.05$ and the magnitude of the maximum velocity $u_{\max}$, and diffusive transport

$$\Delta t_{\mathrm{visc}} = \alpha_{\mathrm{visc}}\frac{L_0^2}{\nu_{\max}} \tag{15}$$

with $\alpha_{\mathrm{visc}} = 0.0625$ and the maximum kinematic viscosity $\nu_{\max}$. The maximum time step allowed is

$$\Delta t = \min\left(\Delta t_{\mathrm{CFL}}, \Delta t_{\mathrm{visc}}\right). \tag{16}$$

3.2 s-IISPH

In highly viscous flow, the time step is commonly limited by the stability criterion for diffusive transport (Eq. (15)). To overcome this limitation, we replace the explicit

time integration (Eq. (11)) in the predictor step by an implicit time integration. The position of particles remains unchanged during time integration of the velocity. Therefore, we implicitly assume that the relative configuration of the particles in a time step is constant. This enables us to formulate a linear problem. As a result, we expect small errors for transient flow but accurate steady-state solutions.

The intermediate velocity, using an implicit Euler step, is

$$\mathbf{u}_i^{*,t+\Delta t} = \mathbf{u}_i^t + \left[\frac{1}{\rho}\left(\mu\Delta\mathbf{u} + \mathbf{F}\right)_i\right]^{t+\Delta t, x^t} \Delta t. \tag{17}$$

Note that the superscript of the acceleration changes from t to $t + \Delta t$. The PPE (Eq. (10)) doesn't change. In the corrector step, we can either directly use equation (12) or calculate the new velocity with another implicit step

$$\mathbf{u}_i^{t+\Delta t} = \mathbf{u}_i^t + \left[\frac{1}{\rho}\left(\mu\Delta\mathbf{u} + \mathbf{F} - \nabla p\right)_i\right]^{t+\Delta t, x^t} \Delta t. \tag{18}$$

Finally, the position of particles $\mathbf{x}_i^{t+\Delta t}$ is updated using equation (13). The unknown quantities per particle are the intermediate velocity $\mathbf{u}_i^{*,t+\Delta t}$ (necessary to solve the PPE), the pressure of the particles p_i and the integrated velocity $\mathbf{u}_i^{t+\Delta t}$. Therefore the problem size is $N \cdot (2D + 1)$ with the dimension D and the total particle number N. To solve equations (17), (10) and (18), three linear equation systems (LES) of sizes $N \cdot D$, N and $N \cdot D$ are formulated and solved consecutively. The properties of the matrix of the LES are similar to the PPE in ISPH and therefore the same solver can be used.

Since the position of particles is integrated explicitly using equation (13) we restrict the time step size to equation (14).

3.3 f-IISPH

In the previous section, an implicit time integration scheme for velocity of particles was presented. A major assumption was the constant relative configuration of particles, which is not valid for transient flow with curved streamlines. Here, we formulate an extension of the s-IISPH approach to a fully implicit time integration scheme, which includes velocity and position of particles.

The intermediate velocity is now calculated at a future position

$$\mathbf{u}_i^{*,t+\Delta t} = \mathbf{u}_i^t + \left[\frac{1}{\rho}\left(\mu\Delta\mathbf{u} + \mathbf{F}\right)_i\right]^{t+\Delta t, x^{t+\Delta t}} \Delta t. \tag{19}$$

Note that the superscript of the acceleration changes from x^t to $x^{t+\Delta t}$. As before, the PPE (Eq. (10)) doesn't change. In the corrector step, the new velocity is

$$\mathbf{u}_i^{t+\Delta t} = \mathbf{u}_i^t + \left[\frac{1}{\rho}\left(\mu\Delta\mathbf{u} + \mathbf{F} - \nabla p\right)_i\right]^{t+\Delta t, x^{t+\Delta t}} \Delta t. \tag{20}$$

The position of particles $\mathbf{x}_i^{t+\Delta t}$ is updated iteratively using

$$\mathbf{x}_i^{t+\Delta t} = \mathbf{x}_i^t + \frac{\mathbf{u}_i^t + \mathbf{u}_i^{t+\Delta t}}{2}\Delta t. \tag{21}$$

The unknown quantities per particle are now the intermediate velocity $\mathbf{u}_i^{*,t+\Delta t}$, the pressure of the particles p_i, the integrated velocity $\mathbf{u}_i^{t+\Delta t}$ and the integrated position $\mathbf{x}_i^{t+\Delta t}$. Since the kernel function is a non-linear function we cannot formulate a linear problem. Therefore we use the LES of Section 3.2 inside of a fixed point iteration for the position of the particles. Thus, we iteratively solve the LES of equations (19), (10) and (20) with sizes $N \cdot D$, N and $N \cdot D$ and update the position after every loop k according to equation (21). The iteration tolerance

$$\epsilon < \frac{1}{N} \sum_i \frac{|\mathbf{x}_i^{t+\Delta t,k+1} - \mathbf{x}_i^{t+\Delta t,k}|}{|\mathbf{x}_i^{t+\Delta t,k}|} \tag{22}$$

is set to 2×10^{-5}. Initially, we guess the new position based on the previous velocity using equation (21) with $\mathbf{u}_i^{t+\Delta t,x^{t+\Delta t},k=0} = \mathbf{u}_i^{t,x^t,k=0}$. To approximate accuracy we use an empirical error estimator and reduce or increase the time step size, where a time step is bisected if the deviation in position after the first iteration error is larger than 6×10^{-5} and doubled if the the error is lower than 10^{-5}. Since this approach is fully implicit we do not apply any other time step restriction. Nevertheless, the time step should not be too large because solutions could be inaccurate, as well known for implicit schemes.

4 Results

In this section, we compare ISPH, s-IISPH and f-IISPH schemes using a Poiseuille flow, Rayleigh–Taylor instability and Taylor–Green vortex in 2D to investigate accuracy of the schemes.

4.1 Poiseuille flow

Poiseuille flow is a common test case to validate implementations and show convergence for incompressible fluids because an analytic solution of the flow profile is known. We consider a single-phase, 2D channel of size $L \cdot L$ with $L = 1\,\text{mm}$. The density of the fluid is $\rho = 1000\,\text{kg}\,\text{m}^3$. Infow/outflow boundary conditions are applied with a pressure gradient of $\Delta p = 0.012\,\text{Pa}$ in flow direction. At the wall of the channel no-slip boundary conditions are used. In the following, we investigate a Reynolds number $\text{Re} = 0.01$, corresponding to a dynamic viscosity $\mu = 0.01\,\text{Pas}$. The Reynolds number is defined as

$$\text{Re} = \frac{\rho u_{\text{ref}} L}{\mu} \tag{23}$$

with the reference velocity $u_{\text{ref}} = \frac{2}{3} u_{\max}$ as the average velocity. We choose a numerical resolution of 50 particles per channel width, corresponding to a Cartesian initial particle distance $L_0 = 0.02\,\mu\text{m}$. Note that in the implicit schemes, steady-state could be achieved using one very large time step. Here, we use an initial time step size of the implicit schemes $\Delta t = 10^{-3}$. In s-IISPH the time step is constant during simulation. In f-IISPH the time step size first decreases by an order of magnitude in the first time step and then increases again to the order of 10^{-3}.

In Figure 1, we show the dimensionless velocity profile $u^* = u_x/u_{\text{ref}}$ over the width of the channel $y^* = y/L$ for $\text{Re} = 0.01$ at steady-state.

We find good agreement of the velocity profile of ISPH, s-IISPH and f-IISPH with the analytic solution for laminar Poiseuille flow. The error of the maximum velocity of each algorithm is summarized in Table 1.

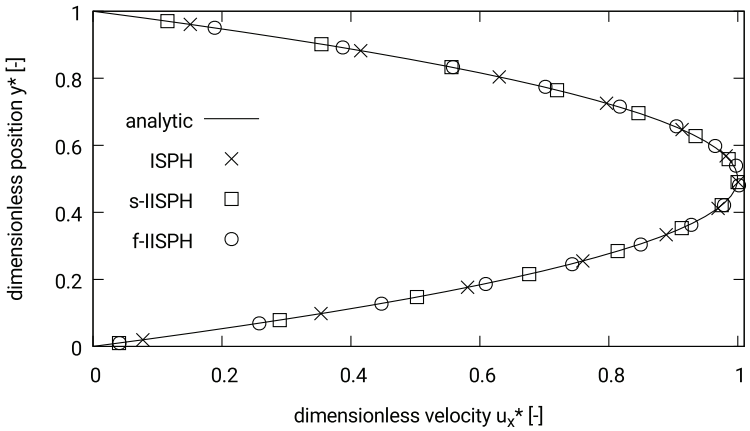

Fig. 1. Dimensionless velocity profile of Poiseuille flow in 2D channel at steady-state for Re = 0.01. ISPH, s-IISPH and f-IISPH are marked by symbols. Solid line represents analytic solution.

Table 1. Summary relative error in maximum of velocity for Poiseuille flow at steady-state with reference to the analytic solution and a resolution of $L_0 = 0.02\,\mu$m in a 2D channel.

Algorithm	Error [%]
ISPH	0.1
s-IISPH	0.11
f-IISPH	0.08

The error of the maximum velocity is generally low in all algorithms, but slightly lower in the fully implicit scheme. We conclude that all schemes are implemented correctly.

4.2 Rayleigh–Taylor instability

Rayleigh–Taylor instability (RTI) is a common test case for multiphase flow with surface tension. RTI was discussed in detail in literature, e.g. [12,31,38–41]. It was shown that the dynamics of RTI are well captured in SPH simulations. In this section we investigate the implicit time integration schemes in RTI and compare the tip position over time with ISPH.

We choose the same setup of a single mode RTI as in [41]. Two fluids are layered in a closed box of size $L_x = 1\,\mathrm{m}$ and $L_y = 4\,\mathrm{m}$. The upper region ($y > 2L_x$) is filled with fluid 2 ($\rho_2 = 2000\,\mathrm{kg\,m^3}$, $\nu_2 = 10^{-3}\,\mathrm{m^2\,s^{-1}}$) and the lower region ($y < 2L_x$) is filled with fluid 1 ($\rho_1 = 1000\,\mathrm{kg\,m^3}$, $\nu_1 = 10^{-3}\,\mathrm{m^2\,s^{-1}}$). The gravity is $g = 0.09\,\mathrm{m^2\,s^{-1}}$ directed in negative y coordinate. Initially, all particles are in regular Cartesian order ($L_0 = 0.0125\,\mathrm{m}$) and we impress a sinusoidal perturbation as described in [41]

$$y = 2 + \zeta_0 \cos\,(kx) \tag{24}$$

with $\zeta_0 = 0.05L_x$, $k = 2\pi/\lambda$ and $\lambda = 1\,\mathrm{m}$. The dimensionless coordinates, time and surface tension are $x^* = x/L_x$, $y^* = y/L_x$, $t^* = t\sqrt{g/L_x}$ and $\phi = \sigma/\sigma_c$ with the critical surface tension $\sigma_c = (\rho_2 - \rho_1)\,\mathrm{g\,k^2}$ when gravitational force is balanced. The surface tension coefficient is $\sigma = 0.9119\,\mathrm{N\,m^{-1}}$ and corresponds to $\phi = 0.4$. In

Fig. 2. Contour of phases of Rayleigh–Taylor instability for $\phi = 0.4$ at times $t^* = 3$ (a–b) and $t^* = 6$ (c–d). Results for ISPH (left half) and s-IISPH (right half in (a) and (c)) and f-IISPH (right half in (b) and (d)).

the implicit time integration schemes, we use an initial time step size of 10^{-3} s, which is in the same range as in ISPH.

The contour of phases is shown in Figure 2.

On the left side of each figure the contour of ISPH and on the right side s-IISPH and f-IISPH, respectively, are shown. In Figure 2 we observe small differences of the shape of the finger and the position of the finger tip between ISPH and s-IISPH. The difference is larger for f-IISPH. The reason is the larger time step of the implicit time integration scheme. It results in a wider finger, especially near the tip, and a lower velocity of the finger.

A quantitative analysis is shown in Figure 3, where the position of the finger tip is shown over time.

The upper and lower positions of the tip of the finger using s-IISPH are slightly higher than in ISPH. In f-IISPH the finger clearly evolves at later time. For larger times, the slopes of all curves in Figure 3 are equal indicating the same dynamics of the finger. The slope of the curve is $\approx 1/3$. This is in the expected range for the numerical simulation compared to [41].

The resulting error from difference of the position of the finger tips is shown in more detail in Figure 4. We consider the difference between maximum and minimum finger tips' position. The error ϵ indicates the difference of distance between s-IISPH or f-IISPH, respectively, and ISPH. Accordingly, ϵ is the relative error with ISPH as a reference.

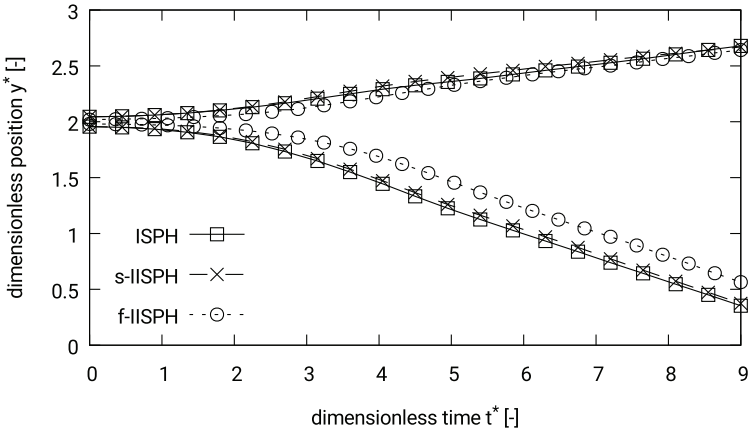

Fig. 3. Evolution of upper and lower finger tips over time for $\phi = 0.4$. Comparison of ISPH, s-IISPH and f-IISPH.

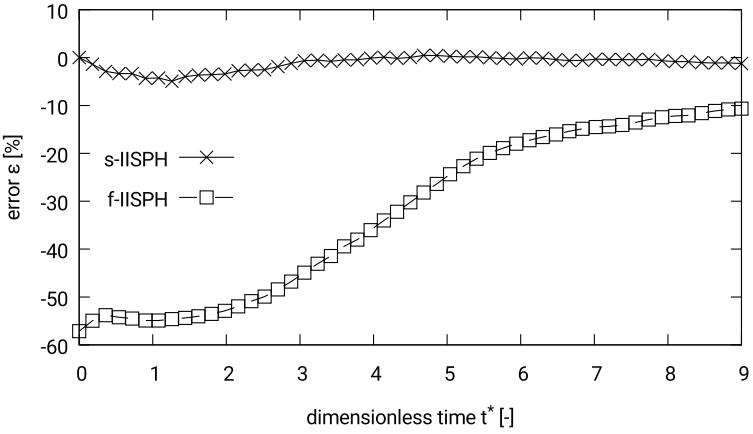

Fig. 4. Deviation of position of upper and lower finger tips over time for $\phi = 0.4$. s-IISPH and f-IISPH indicate the difference between s-IISPH and f-IISPH to ISPH, respectively.

We observe that the difference of the position of the finger tips in s-IISPH is very small. Mainly at early times errors up to 5% are present because of larger time step size and therefore the smoothing effect of the implicit time integration. The error for f-IISPH is much larger, up to 60%, and reduces over time. The reason is that the time step size is much larger in the beginning of the simulation and smooths out some dynamics which leads to deviations of the propagation of the fluid interface. This is shown in Figure 5.

The first time step size is small and approximately 50 iterations are necessary to satisfy the integration tolerance. Then, the time step size increases up to $\Delta t^* = 0.03$ with only a few iterations. With ongoing time the iterations increase up to approx. 20 before the time step size is bisected. The reason is the rising vortex at finger formation where the gradient of velocity between time steps increases. At later times, when the finger is developed a more uniform velocity distribution enables fewer iterations to satisfy the integration tolerance.

We conclude that, while the dynamics of RTI is reproduced well by the implicit solvers, errors in the accuracy of interface propagation are present that originate

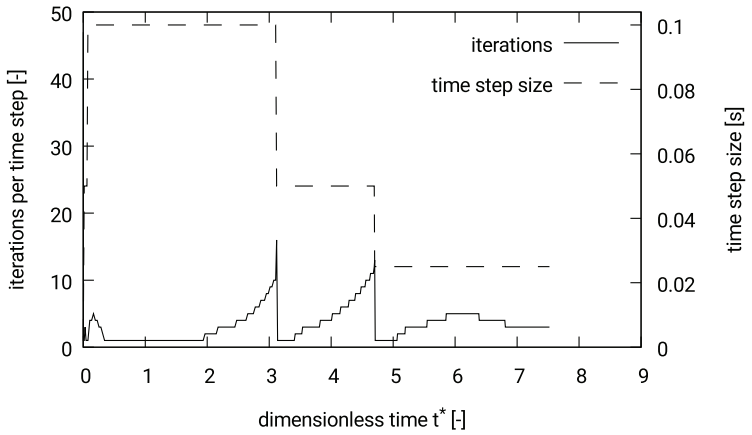

Fig. 5. Variation of iterations per time step and time step size over dimensionless time for f-IISPH.

mainly from the larger time step size. In addition, it is found that both implicit time integration schemes prove to be numerically stable.

4.3 Taylor–Green flow

An appropriate test case to analyze numerical damping of implicit time integration schemes is two-dimensional Taylor–Green flow. This test case is well discussed in literature, e.g. [42]. The dimensionless kinetic energy of the system is

$$E^*_{\mathrm{kin}} = \frac{E_{\mathrm{kin}}}{E_{\mathrm{kin},0}} = \exp(-16\pi^2 \nu t), \tag{25}$$

with the initial kinetic energy $E_{\mathrm{kin},0}$ and the kinematic viscosity ν, which allows to validate energy conservation of algorithms. We consider a Reynolds number $\mathrm{Re} = \frac{L u_{\max}}{\nu} = 100$ with characteristic length $L = 1\,\mathrm{m}$, the maximum initial velocity $u_{\max} = 1\,\mathrm{m\,s^{-1}}$, periodic boundary conditions and a resolution $L_0 = 0.01\,\mathrm{m}$. The initial divergence-free velocity field is

$$u^*_x = \sin(2\pi x^*)\cos(2\pi y^*), \tag{26}$$
$$u^*_y = -\cos(2\pi x^*)\sin(2\pi y^*). \tag{27}$$

The dimensionless velocities are $u^*_x = u_x/u_{\max}$ and $u^*_y = u_y/u_{\max}$, respectively, and the dimensionless coordinates are $x^* = x/L$ and $y^* = y/L$, respectively.

In Figure 6, we exemplify the pressure distributions and magnitude of velocity for $\mathrm{Re} = 100$ at $t^* = 1.5$.

The pressure and velocity distribution for ISPH, s-IISPH and f-IISPH are almost identical.

In Figure 7 the decay of kinetic energy over time compared to the analytic solution (Eq. (25)) for ISPH, s-IISPH and f-IISPH is shown.

We observe that the decay of kinetic energy is well captured in all time integration schemes. Nevertheless, small deviations from the analytic solution are found. These deviations are analyzed in Figure 8, considering the relative error of the kinetic energy with reference to the analytic solution.

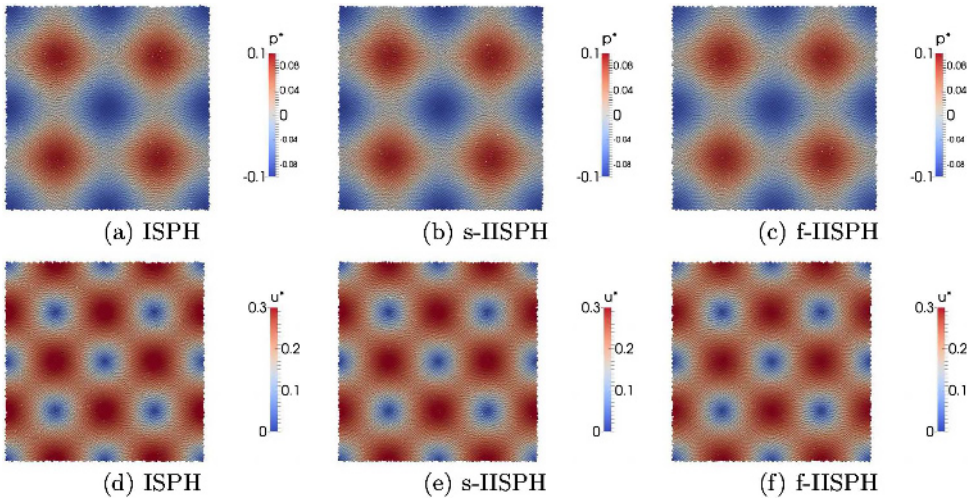

Fig. 6. Contour of pressure (top row) and magnitude of velocity (bottom row) in Taylor–Green flow for Re = 100 at time $t^* = 1.5$. The dimensionless velocity and pressure are $u^* = u/u_{\max}$ and $p^* = p/(\rho u_{\max}^2/2)$. The resolution is $L_0 = 0.01\,\mathrm{m}$.

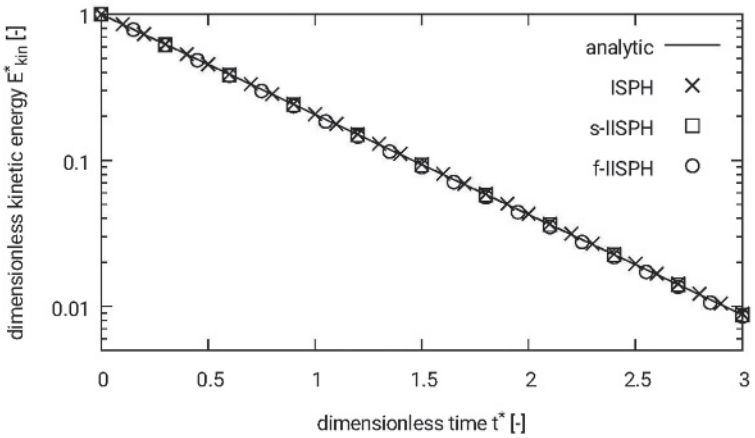

Fig. 7. Decay of kinetic energy in Taylor–Green flow over time for ISPH, s-IISPH and f-IISPH at Re = 100. The resolution is $L_0 = 0.01\,\mathrm{m}$.

In ISPH, we observe a linear increase of the error of kinetic energy over time. The reason is that in ISPH an explicit Euler step is used, which does not conserve energy. As shown in other literature, e.g. [42], this can be reduced by increase of resolution. In s-IISPH, the kinetic energy is underestimated at the beginning and increases again over time. The underestimation of energy may be a result of the smoothing effect of the implicit scheme, which is typically known for single step integration schemes. In f-IISPH, we observe a larger underestimation of kinetic energy. This is in agreement with previous findings and demonstrates that in the fully implicit time integration scheme numerical dissipation is large, originating from larger time step sizes. Again, the implicit time integration schemes prove to be numerically stable. With up to 5 iterations of position per time step on average in f-IISPH, the computational cost is only an order of magnitude larger compared to s-IISPH. Nevertheless, improvements to account for accuracy, e.i. error estimators, are needed.

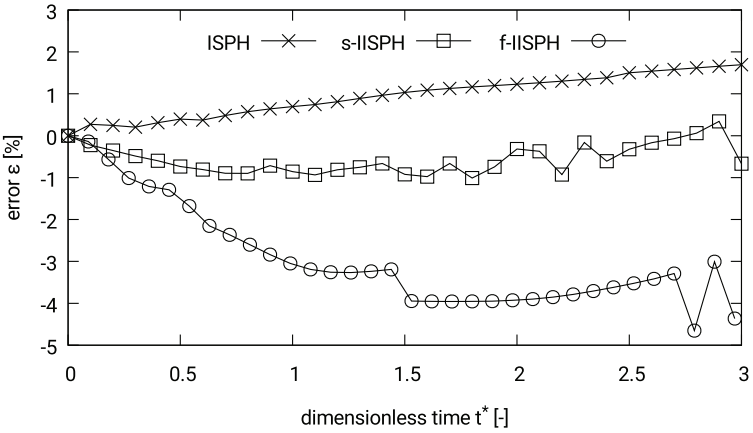

Fig. 8. Relative error, with reference to the analytic solution, in kinetic energy in Taylor–Green flow over time for ISPH, s-IISPH and f-IISPH at Re = 100. The resolution is $L/L_0 = 100$.

5 Conclusion

In this article we studied two different implicit time integration schemes in truly incompressible Smoothed Particle Hydrodynamics. In one time integration scheme, s-IISPH, only velocity is integrated implicitly while the position of particles remain constant and are updated at the end of a time step. In a second scheme, f-IISPH, we integrate both velocity and position simultaneously using a linear equation system for velocity embedded in a fixed point iteration for position update.

We investigated Poiseuille flow to validate accurate implementation of the integration schemes. In all integration schemes, good agreement of the velocity profile to the analytic solution for laminar channel flow is found. Afterwards, Rayleigh–Taylor instability is investigated. The s-IISPH scheme agrees reasonably well to the reference solution of ISPH while f-IISPH shows large deviations for transient flow. We quantitatively analyzed the position of finger tips and found up to 60% deviation between f-IISPH and ISPH. The reason for this deviation is the up to 10 times larger time step. Finally, we studied a 2D Taylor–Green vortex to analyze the energy conservation of the integration schemes. We found that, while in ISPH a linear error in kinetic energy propagates due to explicit time integration, the implicit schemes underestimate the kinetic energy. Again, the error in f-IISPH is larger than in s-IISPH due to the larger time step size.

In future work higher order integration schemes, e.g. Crank–Nicolson or Runge–Kutta schemes, should be investigated to improve accuracy. Another improvement may be an error estimator to ensure accuracy. In some applications, e.g. in molding flow or micro devices, the larger computational cost of an implicit scheme outperforms explicit integration schemes and, therefore, are worth to improve for real-life applications.

The work is supported by the German Research Foundation (DFG). The authors acknowledge financial support within the Collaborative Research Center 716.

Author contribution statement

M. Hopp-Hirschler worked out the implicit time integration scheme, numerical implementations and results which are presented in this article. U. Nieken is the supervisor and contributed during discussions and proof-reading of the article.

References

1. R.A. Gingold, J.J. Monaghan, Mon. Not. R. Astron. Soc. **181**, 375 (1977)
2. L.B. Lucy, Astron. J. **82**, 1013 (1977)
3. M. Shadloo, G. Oger, D. Le Touzé, Comput. Fluids **136**, 11 (2016)
4. M. Hopp-Hirschler, U. Nieken, J. Membr. Sci. **564**, 820 (2018)
5. M. Hirschler, P. Kunz, M. Huber, F. Hahn, U. Nieken, J. Comput. Phys. **307**, 614 (2016)
6. M. Hopp-Hirschler, M.S. Shadloo, U. Nieken, Comput. Fluids **176**, 1 (2018)
7. D. Barcarolo, D.L. Touz, G. Oger, F. de Vuyst, J. Comput. Phys. **273**, 640 (2014)
8. R. Vacondio, B. Rogers, P. Stansby, P. Mignosa, J. Feldman, Comput. Methods Appl. Mech. Eng. **256**, 132 (2013)
9. J. Feldman, J. Bonet, Int. J. Numer. Methods Eng. **72**, 295 (2010)
10. F. Spreng, D. Schnabel, A. Mueller, P. Eberhard, Comput. Part. Mech. **1**, 131 (2014)
11. X. Xu, P. Yu, J. Non-Newtonian Fluid Mech. **229**, 27 (2016)
12. S.J. Cummins, M. Rudman, J. Comput. Phys. **152**, 584 (1999)
13. J.J. Monaghan, J. Comput. Phys. **138**, 801 (1997)
14. S. Litvinov, M. Ellero, X. Hu, N. Adams, J. Comput. Phys. **229**, 5457 (2010)
15. P. Espanol, M. Revenga, Phys. Rev. E **67**, 026705 (2003)
16. X.-J. Fan, R. Tanner, R. Zheng, J. Non-Newtonian Fluid Mech. **165**, 219 (2010)
17. Y. Han, H. Qiang, Q. Huang, J. Zhao, Sci. China Technol. Sci. **56**, 2480 (2013)
18. Y.-W. Han, H.-F. Qiang, H. Liu, W.-R. Gao, Acta Mech. Sin. **30**, 37 (2014)
19. T. Takahashi, Y. Dobashi, I. Fujishiro, T. Nishita, M.C. Lin, Eurographics **34**, 493 (2015)
20. M. Weiler, D. Koschier, M. Brand, J. Bender, Comput. Graph. Forum **37**, 145 (2018)
21. M. Ihmsen, J. Cornelis, B. Solenthaler, C. Horvath, M. Teschner, IEEE Trans. Visual. Comput. Graphics **20**, 26 (2014)
22. J. Cornelis, M. Ihmsen, A. Peer, M. Teschner, Comput. Graph. Forum **33**, 255 (2014)
23. P. Goswami, A. Eliasson, P. Franzén, Implicit incompressible SPH on the GPU, in *Workshop on Virtual Reality Interaction and Physical Simulation VRIPHYS, 2015*
24. R. Rook, M. Yildiz, S. Dost, Numer. Heat Transfer, Part B: Fundam.: Int. J. Comput. Method. **51**, 1 (2007)
25. P.V. Liedekerke, B. Smeets, T. Odenthal, E. Tijskens, H. Ramon, Comput. Phys. Commun. **184**, 1686 (2013)
26. W. Pan, K. Kim, M. Perego, A.M. Tartakovsky, M.L. Parks, J. Comput. Phys. **334**, 125 (2017)
27. J.J. Monaghan, Annu. Rev. Astron. Astrophys. **30**, 543 (1992)
28. M.B. Liu, G.R. Liu, Arch. Comput. Method. Eng. **17**, 25 (2010)
29. J. Bonet, T.-S.L. Lok, Comput. Method. Appl. Mech. Eng. **180**, 97 (1999)
30. J.P. Morris, Int. J. Numer. Methods. Fluids **33**, 333 (2000)
31. S. Shao, E.Y.M. Lo, Adv. Water Resour. **26**, 787 (2003)
32. R. Falgout, A. Cleary, J. Jones, E. Chow, V. Henson, C. Baldwin, P. Brown, P. Vassilevski, U.M. Yang, Hypre Web page (2016), http://acts.nersc.gov/hypre
33. S. Balay, S. Abhyankar, M.F. Adams, J. Brown, P. Brune, K. Buschelman, L. Dalcin, V. Eijkhout, W.D. Gropp, D. Kaushik, M.G. Knepley, L.C. McInnes, K. Rupp, B.F. Smith, S. Zampini, H. Zhang, H. Zhang, PETSc Web page (2016), http://www.mcs.anl.gov/petsc, version 3.3
34. R. Xu, P. Stansby, D. Laurence, J. Comp. Phys. **228**, 6703 (2009)
35. S.J. Lind, R. Xu, P.K. Stansby, B.D. Rogers, J. Comp. Phys. **231**, 1499 (2012)
36. P. Kunz, M. Hirschler, M. Huber, U. Nieken, J. Comput. Phys. **326**, 171 (2016)
37. M. Huber, F. Keller, W. Sckel, M. Hirschler, P. Kunz, S. Hassanizadeh, U. Nieken, J. Comput. Phys. **310**, 459 (2016)
38. A.M. Tartakovsky, P. Meakin, J. Comput. Phys. **207**, 610 (2005)
39. X.Y. Hu, N.A. Adams, J. Comput. Phys. **227**, 264 (2007)
40. N. Grenier, M. Antuono, A. Colagrossi, D. Le Touzé, B. Alessandrini, J. Comput. Phys. **228**, 8380 (2009)
41. M.S. Shadloo, A. Zainali, M. Yildiz, Comput. Mech. **51**, 699 (2012)
42. G. Oger, S. Marrone, D. Le Touzé, M. de Leffe, J. Comput. Phys. **313**, 76 (2016)